Available online at www.sciencedirect.com
ScienceDirect
Catalysis Today 131 (2008) 513–519
CATALYSIS TODAY
www.elsevier.com/locate/cattod

CO oxidation and oxygen-assisted CO adsorption/desorption on Ag/MnO_x catalysts

Rongrong Hu [a], Lanying Xie [b], Shi Ding [a], Jian Hou [a], Yi Cheng [a], Dezheng Wang [a,*]

[a] *Department of Chemical Engineering, Tsinghua University, Beijing 100084, China*
[b] *Research Center, Changde Cigarette Manufacture Company, Tongyan Road West, Changde, Hunan 415000, China*

Available online 28 November 2007

Abstract

A series of Ag-doped manganese oxide catalyst were synthesized by the reflux method in an acid medium. The surface structure of the catalysts was characterized by N_2 adsorption, XRD and TEM experiments. The catalysts showed excellent catalytic activity for CO oxidation. The adsorption and oxidation of CO on a 1.0% Ag/MnO_x catalyst between 393 and 493 K were studied by means of single pulse experiments in a TAP reactor. The adsorption of CO was reversible at these temperatures and CO_2 was formed in an oxidation reaction of CO and lattice oxygen. Curve fitting to the experimental TAP response curves of the reactant and product was used to determine the kinetic parameters for the elementary steps. The activation energies were 83 kJ/mol for CO desorption, 31 kJ/mol for CO_2 desorption, and 116 kJ/mol for the surface CO oxidation by lattice oxygen. In addition, the effect of coadsorbed O_2 on CO adsorption was studied by the TAP technique. Below 353 K, there was a sharp increase, by about one order of magnitude, in the rate constant of CO adsorption promoted by the presence of coadsorbed O_2.

Keywords: CO oxidation; CO adsorption; Ag-doped manganese oxide catalyst; Metal oxide catalyst; TAP

1. Introduction

CO oxidation is of practical importance for controlling the CO poison that can come from incomplete combustion processes, e.g. cigarette combustion. A CO oxidation catalyst has to be added to complete the combustion to remove the poison. The reaction mechanism for CO oxidation over reduced metals is one of the best researched in surface science, but in many situations, it is not possible to maintain a reduced surface, e.g. with catalysts that get exposed to the atmosphere, and it is an oxide surface that is the catalyst. Due to this, and also because many metals are active only in a limited range of CO and O_2 compositions and are inactive under conditions of excess CO and excess O_2, it is of interest to study CO oxidation on metal oxides for applications where catalyst exposure to the atmosphere is unavoidable. The reaction mechanism over an oxide surface is much less understood than that over reduced metals, but already known to possess a very rich surface chemistry [1] and synergism effects where a multicomponent catalyst – metal oxide and reducible metal – has the highest activity [2].

Among the catalysts that are resistant to exposure to the atmosphere, Au/TiO_2 is one of the best catalyst [3,4], but its activity is highly dependent on preparation conditions and it also needs *in situ* pretreatment to be highly active [5–7]. In contrast, Hopcalite-type manganese oxide-based catalysts are more easily prepared and are quite active [8,9]. These catalysts can be made even more active when the manganese oxide is prepared in the form of octahedral molecular sieves (OMS), esp. OMS-2 loaded with metals [10]. Although many noble metals, including Ag [11], Pd [12,13], Pt [14,15] and Ru [16], loaded on metal oxides have been studied, it appears that OMS-2 loaded with Ag [10] is especially active. The aim of this work is to provide more data and information on the detailed kinetics on these potentially useful Ag-doped MnO_x catalysts and further discuss the reaction mechanism for the oxidation of CO.

It is widely agreed that the oxidation of CO on supported group 8–10 metal catalysts, such as Pt, Pd and Ru, follows a Langmuir-Hinshelwood mechanism [17,18]. That is, the surface reaction occurs between adsorbed CO and dissociatively adsorbed oxygen. However, uncertainty and debate remain in the CO oxidation mechanism of Au and Ag catalysts,

* Corresponding author. Fax: +86 10 62772051.
E-mail address: wangdz@flotu.org (D. Wang).

0920-5861/$ – see front matter © 2007 Elsevier B.V. All rights reserved.
doi:10.1016/j.cattod.2007.10.023

Nomenclature

A_i	preexponential factor (s^{-1})
C_i	gas phase concentration of component i (mol/m^3)
$C_{i,ads}$	surface concentration of adsorbed species i on catalyst (mol/m^3)
C^0	active site concentration of catalyst (mol/m^3)
$C_{[O]}$	surface concentration of the support lattice oxygen, 1.0 mol/m^3
D_i	effective diffusivity of component i (m^2/s)
E	activation energy (kJ/mol)
k_{ads}	adsorption rate constant (m^3/kg s)
k_{des}	desorption rate constant (s^{-1})
k_{srxn}	surface reaction rate constant (m^3/kg s)
L	reactor bed length (m)
$N_{P,i}$	amount of species i in the input pulse (mol)
t	time variable (s)
T	temperature (K)
x	space variable in the reactor (one-dimensional model) (m)

Greek letters

$\delta(t-\tau)$	Dirac function (at time τ), dimensionless
ε	bed void density, dimensionless
ρ_b	catalyst bed density (kg/m^3)

especially when they are supported on reducible transition metal oxides such as Fe_2O_3, TiO_2, NiO and MnO_x because of the possible ability of the ''active'' oxides to provide reactive oxygen. One focus of researchers is the role of the oxygen species. For example, Gupta and Tripathi [19,20] reported that CO oxidation occurred via a normal redox mechanism of oxygen abstraction from the Fe_2O_3 lattice on their Au/Fe_2O_3 samples. A TAP study by Olea et al. [21,22] reported that the CO_2 yield smoothly decreased with increasing delay between the O_2 ''pump'' and the CO ''probe'' pulses and they excluded a contribution from support lattice oxygen for their calcined Au/$Ti(OH)_4$ catalysts. The work of Grisel and Nieuwenhuys [23] indicated that MnO_x is able to activate O_2 and the activated O species not only reacts with adsorbed CO but also replenishes O vacancies that were formed from the reaction of support lattice oxygen and adsorbed CO on the surface of their Au/MnO_x catalysts.

In this work, the CO oxidation mechanism on a series of Ag/MnO_x catalysts was investigated by the temporal analysis of products (TAP) technique. The kinetic parameters of the elementary reaction steps for CO oxidation were obtained, and a previously unreported phenomenon in the reaction mechanism, namely, oxygen-assisted CO adsorption was observed.

2. Experimental

2.1. Sample preparation

The Ag/MnO_x catalysts were synthesized by the reflux method. 3 mL concentrated HNO_3 was added into 30 mL of 0.5 M $MnSO_4 \cdot H_2O$ solution at room temperature to provide an aqueous reaction medium having a pH of 1.0. The solution was then added dropwise into 100 mL aqueous solution containing 5.89 g $KMnO_4$ and an appropriate amount of $AgNO_3$. The resulting black precipitate was stirred vigorously and refluxed at 373 K for 48 h. The solid obtained was filtered and washed with distilled water, followed by drying at 393 K for 6 h and calcination at 573 K in static air.

The series of catalysts prepared include 0.5, 1.0, 1.5 and 2.0% Ag/MnO_x. The loading values are nominal loadings. In this report, we mainly discuss the results from the 1.0% Ag/MnO_x catalyst, which was the best catalyst.

2.2. Physical and chemical characterization

N_2 adsorption/desorption experiments at liquid nitrogen temperature for surface area and pore size distribution (PSD) measurements were performed on a high resolution gas adsorption manometry system further equipped with a 0.1 Torr range Type 120 Baratron (MKS Corporation, USA) for increased precision at very low pressures [24]. Before measurement, the sample was degassed at 573 K for 15 h. Specific surface areas were calculated by the BET method. The PSDs were obtained by calculations using the Horvath–Kawazoe (HK) method using isotherms measured in the low pressure range of 10^{-4} to 10^{-1} Torr to characterize the micropores.

TEM observations were performed with a JEOL JEM-2010 electron microscope. X-ray powder diffraction (XRD) patterns were recorded with a D/Max-2500/PC powder diffractometer (Rigaku, Japan) operated at 40 kV and 250 mA, using nickel-filtered Cu Kα ($\lambda = 0.15418$ nm) radiation.

2.3. Catalytic activity measurements

The material was tested for CO oxidation using a flow fixed bed laboratory microreactor at atmospheric pressure equipped with an online mass spectrometer so that it can be operated as a temperature scanning reactor. Typically, CO, O_2 and the carrier gas argon were fed to the reactor at controlled feed rates using three mass flow controllers. Reactions were carried out using a flow rate of 19 cm^3/min (GHSV = 10,000 h^{-1}) and a gas composition of O_2:CO:Ar = 1:1:10 mol ratio. The amount of catalyst used was about 200 mg. The temperature used was from 293 to 573 K. The products were analyzed using an online CIS 200 mass spectrometer (Stanford Research Systems, USA) and a G7890 gas chromatograph equipped with TCD and FID detectors (Techcomp, China).

2.4. TAP single pulse experiments

TAP single pulse experiments with CO/Ar or CO_2/Ar pulses were carried out in a reactor based on the TAP reactor described by Gleaves et al. [25]. This equipment has been described in previous work [26,27]. The 1.0% Ag/MnO_x CO oxidation catalyst sample was placed as a 6 mm packed bed held in place by wire screens in a 4 mm i.d., 110 mm long tube. The detector was two RGA 200 quadrupole mass spectrometers

factory-modified to use external fast response current amplifiers (SRS, USA) placed in a cylindrical vacuum chamber of 30 cm diameter and 57 cm long that was flanged to the entrance of a 1500 l/s turbomolecular pump. Collected data were usually signal averaged over five pulses.

In the reactor simulation and parameter estimation, the numerical integration of the partial differential equations used a finite volume algorithm based on the Crank-Nicholson scheme. Parameter fitting was usually performed with a genetic evolution optimization algorithm, but was also sometimes performed manually using visual inspection of the curves to optimize the parameters. The accuracy of the numerical computation was verified by halving time and space steps until the computed curves agreed visually. Generally, a space step of 0.1 mm and a time step of 0.01 ms were used.

3. Results and discussions

3.1. N_2 adsorption/desorption isotherms and pore size distribution

A typical isotherm for N_2 adsorption/desorption on the 1.0% Ag/MnO_x material is shown in Fig. 1. The isotherm plots showed steep increases in the low relative pressure range ($P/P_0 < 0.01$), which indicated the presence of micropores. A typical PSD, calculated using the HK method, is shown in the inset in Fig. 1. There was a PSD peak in the range of 4.9–6.6 Å. The sharp profile suggests the existence of a well-defined micropore structure. The BET surface areas of the 1.0% Ag/MnO_x material were measured to be about 80 m^2/g.

3.2. XRD and TEM characterization

The Ag/MnO_x materials synthesized using the reflux method were dark-brown powders. The TEM images clearly showed that they were needle-like nanorods. A typical TEM image is shown in Fig. 2. The diameters of the nanorods ranged from 35 to 50 nm, and the lengths were about 700 nm.

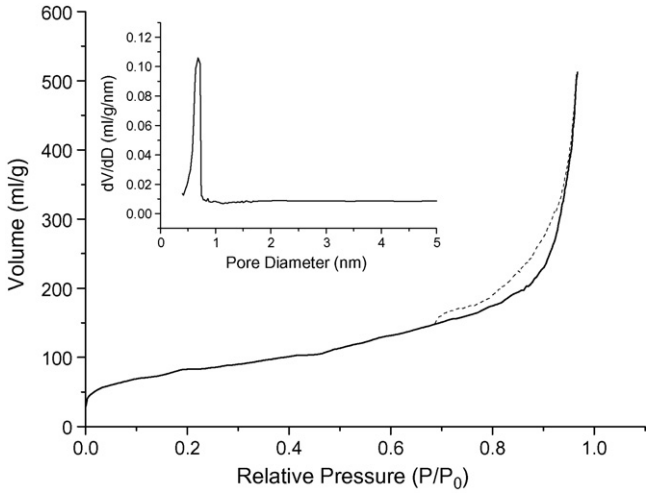

Fig. 1. N_2 adsorption/desorption isotherm and the pore size distribution of the Ag/MnO_x catalyst.

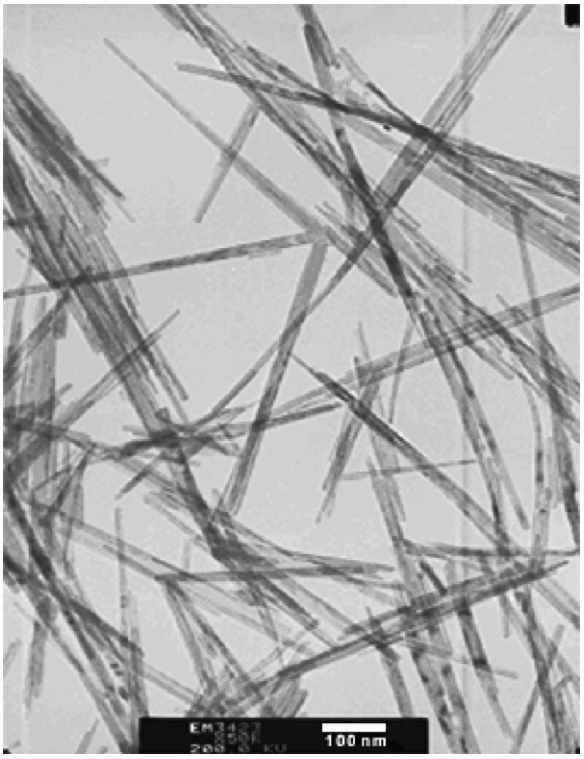

Fig. 2. Typical TEM image of a Ag/MnO_x catalyst.

Fig. 3 shows a typical XRD pattern of the synthesized Ag/MnO_x materials. There were clear main diffraction peaks at $2\theta = 12.6^\circ$, 17.9°, 28.7°, 37.5°, 41.9°, 49.9° and 60.1°, which showed that these have the typical structure of cryptomelane (KMn_8O_{16}, JCPDS 29-1020), that is, the structure of OMS-2 [10]. No peaks related to the dopant Ag metal cations were observed, which indicated that the loaded Ag did not form large particles, but were dispersed in the micropores of the OMS-2 structure. A few samples were characterized by XPS to get information on the oxidation state of Ag and no Ag_2O was seen in the Ag/MnO_x catalysts. More details of the characterization of the Ag/MnO_x materials had been reported elsewhere [28].

3.3. Catalytic activity

The activity characterization by continuous flow experiments at atmospheric pressure and a temperature increase at a rate of 6 K/min from 293 to 573 K is shown in Fig. 4. This shows the conversion of CO over the Ag/MnO_x catalysts as a function of the reaction temperature. MnO_x itself is active but the catalytic activity of MnO_x without Ag is poorer than that of the Ag/MnO_x catalysts. At 413 K, the CO conversion of MnO_x was only 70% when that of the Ag/MnO_x catalysts such as 1.0% Ag/MnO_x had reached 100%. The catalytic activities of 0.5% Ag/MnO_x, 1.0% Ag/MnO_x, 1.5% Ag/MnO_x and 2.0% Ag/MnO_x catalysts for CO oxidation are shown in Fig. 4, which shows that the activity depends on the amount of Ag doped onto the OMS-2. 1.0% Ag/MnO_x catalyst had the best catalytic activity with 100% conversion of CO at a temperature as low as 413 K, and the conversion of CO was already significant even at 320 K.

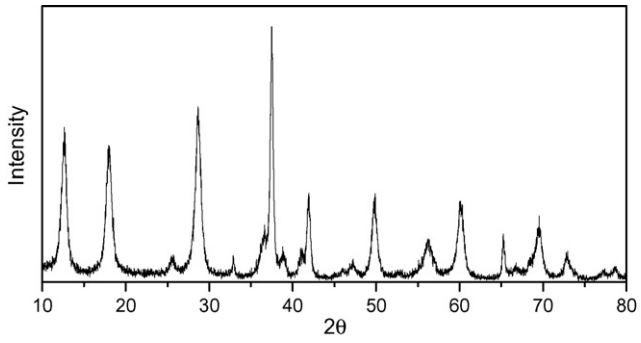

Fig. 3. Typical XRD pattern of a Ag/MnO_x catalyst.

3.4. Adsorption and oxidation of CO

The chemisorption of CO on the 1.0% Ag/MnO_x catalyst was studied by single pulse experiments in a TAP reactor with input pulses of CO/Ar and CO_2/Ar. The results of pulsing CO_2 are shown in Fig. 5. This shows that injecting CO_2 over the catalyst between 293 and 423 K resulted in broadened response curves, which can be seen by comparing the CO_2 and argon response curves. As the temperature increased, the CO_2 responses got sharper. The mass balance using the internal standard, argon, showed that CO_2 was neither irreversibly adsorbed nor converted. The shapes of the CO_2 responses were independent of the pulse size, which confirmed that the transport regime was Knudsen diffusion and that the experiments were performed over surfaces of low surface coverage.

The chemisorption of CO on the 1.0% Ag/MnO_x catalyst showed a different behavior in response to CO/Ar pulse injection. The data are shown in Fig. 6. There was a similarity with the CO_2 results in that a higher temperature gave sharper CO response curves, but a mass balance using the argon internal standard showed that the amount of CO eluted was less than

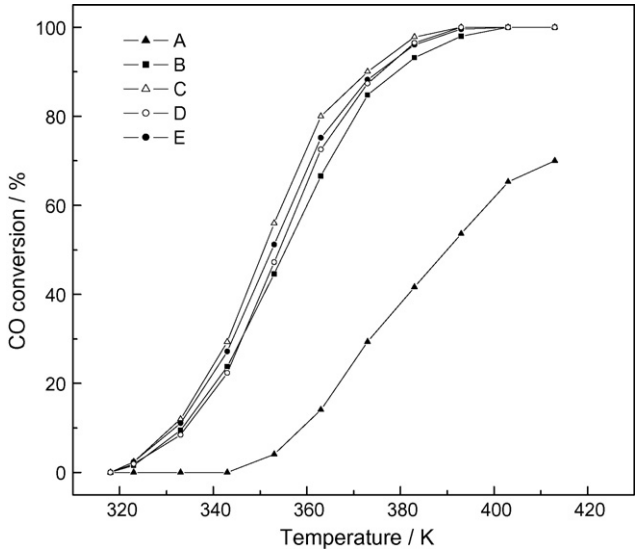

Fig. 4. Temperature dependence of CO conversion over the Ag/MnO_x catalysts. (A) MnO_x; (B) 0.5% Ag/MnO_x; (C) 1.0% Ag/MnO_x; (D) 1.5% Ag/MnO_x and (E) 2.0% Ag/MnO_x (O_2:CO:Ar = 1:1:10, 200 mg catalyst, space velocity = 10,000 h^{-1}).

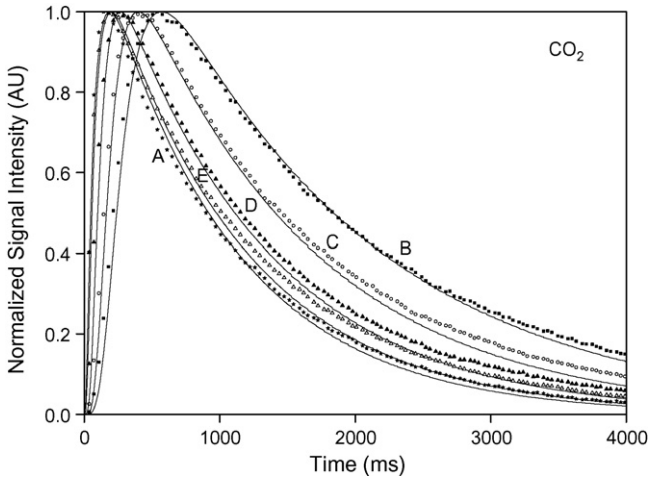

Fig. 5. Experimental (lines) and simulated (symbols) response curves of Ar (A) and CO_2 (B–E) from pulsed Ar/CO_2 over the 1% Ag/MnO_x catalyst. (A) 293 K; (B) 293 K; (C) 323 K; (D) 373 K and (E) 423 K.

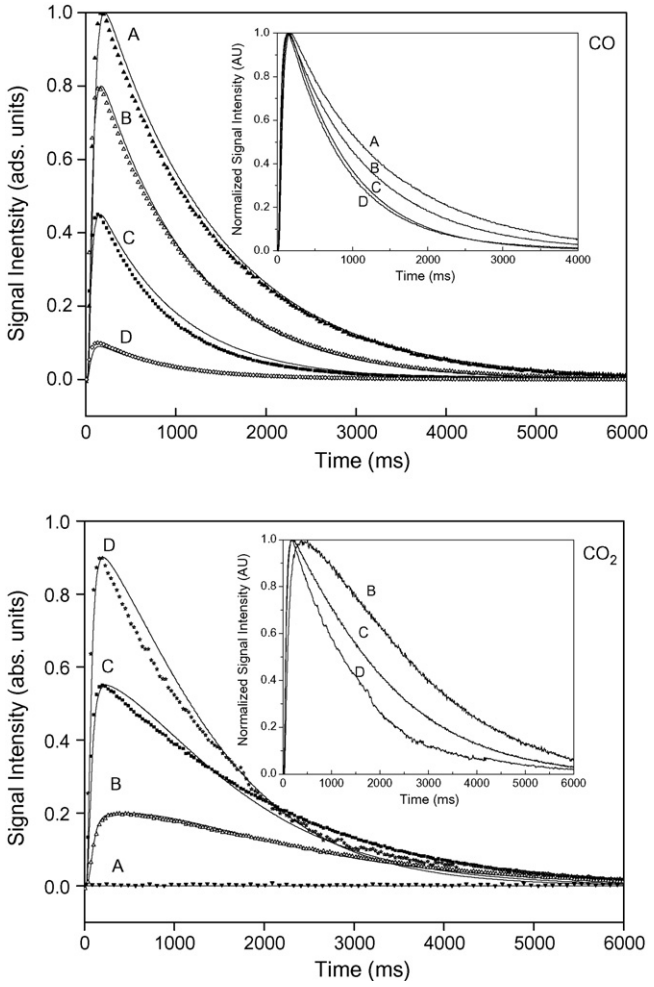

Fig. 6. Experimental (lines) and simulated (symbols) CO and CO_2 response curves from pulsed CO/Ar over the 1% Ag/MnO_x catalyst. (A) 393 K; (B) 423 K; (C) 473 K and (D) 493 K.

injected. At low temperatures, there was irreversible adsorption on the 1.0% Ag/MnO_x catalyst, and there may be some conversion to CO_2 but at a rate that was too slow to give a detectable response curve. When the temperature of the catalyst was increased to 423 K, CO_2 response curves could be detected. The oxygen source for the oxidation of CO was the lattice oxygen of the 1.0% Ag/MnO_x catalyst since no oxygen was fed into the reactor. The oxidation rate of adsorbed CO was dependent on the temperature of the catalyst surface. No CO but only CO_2 was detected at the outlet of the reactor when the temperature was above 493 K, that is, all of the pulsed CO molecules had been converted to CO_2.

Quantitative reaction kinetics parameters and more detailed information about the elementary surface reaction steps for CO oxidation on the 1.0% Ag/MnO_x catalyst were obtained by the modeling of the TAP reactor response curves. The reactor modeling procedure used had been discussed in our previous work [25,26]. The continuity equations in the inert sections are the diffusion equations:

$$\varepsilon \frac{\partial C_i}{\partial t} = \frac{\partial}{\partial x} D_i \frac{\partial C_i}{\partial x} \tag{1}$$

Initial condition:

$$0 < x \le L = \text{vacuum pump entrance},\ t = 0: \quad C_i = 0 \ \text{and}\ C_{i,\text{ads}} = 0, \quad \forall i \tag{2}$$

Boundary conditions (BC) at the entrance and exit of the reactor:

$$x = 0,\ t \ge 0: \quad -D_i \frac{\partial C_i}{\partial x} = \frac{\delta(t-\tau) N_{\text{P},i}}{A_r} \quad (\text{pulsed species}) \qquad = 0 \quad (\text{all other species}) \tag{3}$$

$$x = L = \text{vacuum pump entrance},\ t \ge 0: \quad -D_i A_\text{p} \frac{\partial C_i}{\partial x} = S_\text{p} C_i, \quad \forall i \tag{4}$$

BC (3) assumes that pulse injection is infinitely fast. BC (4) accounts for the situation that the vacuum pump has a finite pumping speed, S_p.

The reactor continuity equations in the catalyst bed section contain the reaction terms of interest. In this work, reactions (5)–(7) were used to describe the elementary reaction steps for CO oxidation on the 1.0% Ag/MnO_x catalyst, where S_1 and S_2 are two different types of active sites on the surface of the catalysts. The experiments here do not provide any data that can be used to deduce the nature of these sites but the general model of adsorption on oxide surfaces can be used to suggest that the S_1 site is probably a metal cation site and O–S_2 is surface lattice oxygen.

$$\text{CO} + \text{S}_1 \underset{k_{\text{des,CO}}}{\overset{k_{\text{ads,CO}}}{\rightleftharpoons}} \text{CO} - \text{S}_1 \tag{5}$$

$$\text{CO} - \text{S}_1 + \text{O} - \text{S}_2 \xrightarrow{k_\text{srxn}} \text{CO}_2 - \text{S}_1 - \text{S}_2 \tag{6}$$

$$\text{CO}_2 - \text{S}_1 - \text{S}_2 \underset{k_{\text{ads,CO}_2}}{\overset{k_{\text{des,CO}_2}}{\rightleftharpoons}} \text{CO}_2 + \text{S}_2 + \text{S}_1 \tag{7}$$

In the TAP experiments, since no oxygen was fed into the reactor, the reactions (5)–(7) used for the modeling of the pulse experiments only accounted for the adsorption, desorption and surface reaction steps of CO and the desorption of CO_2. For the gas species, the CO and CO_2 continuity equations in the catalyst bed section can be written as

$$\varepsilon \frac{\partial C_i}{\partial t} = \frac{\partial}{\partial x} D_{i,\text{bed}} \frac{\partial C_i}{\partial x} - \varepsilon k_{\text{ads},i} C_i (C^0 - C_{\text{CO}_\text{ads}} - C_{\text{CO}_2\text{ads}}) + \rho_\text{b} k_{\text{des},i} C_{i_\text{ads}} \tag{8}$$

For the CO and CO_2 surface species, the reaction kinetics equations in the catalyst bed section, respectively, are:

$$\rho_\text{b} \frac{\partial C_{\text{CO}_\text{ads}}}{\partial t} = \varepsilon k_{\text{ads,co}} C_\text{CO} (C^0 - C_{\text{CO}_\text{ads}} - C_{\text{CO}_2\text{ads}}) - \rho_\text{b} k_{\text{des,co}} C_{\text{CO}_\text{ads}} - \rho_\text{b} k_\text{srxn} C_{\text{CO}_\text{ads}} C_{[\text{O}]} \tag{9}$$

$$\rho_\text{b} \frac{\partial C_{\text{CO}_2\text{ads}}}{\partial t} = \varepsilon k_{\text{ads,CO}_2} C_{\text{CO}_2} (C^0 - C_{\text{CO}_\text{ads}} - C_{\text{CO}_2\text{ads}}) - \rho_\text{b} k_{\text{des,CO}_2} C_{\text{CO}_2\text{ads}} + \rho_\text{b} k_\text{srxn} C_{\text{CO}_\text{ads}} C_{[\text{O}]} \tag{10}$$

k_ads, k_des and k_srxn are the adsorption, desorption and surface reaction rate constants. C^0 is the active site concentration on the catalyst, but because the TAP experiments used very small pulses, the concentrations of adsorbed CO and CO_2 on the 1% Ag/MnO_x catalyst, C_{CO_ads} and $C_{\text{CO}_2\text{ads}}$, were very small and $(C^0 - C_{\text{CO}_\text{ads}} - C_{\text{CO}_2\text{ads}})$ in equations 9 to 12 can be approximated to C^0. Then, the adsorption rate expression contains the rate constant as the product $k_\text{ads}\ C^0$ and the two components cannot be individually determined. $C_{[\text{O}]}$ is the concentration of the lattice oxygen of the catalyst surface O–S_2, which is the oxygen source for the oxidation of CO. It can be considered a constant in the modeling since the lattice oxygen atoms on the catalyst were much more than the pulsed CO molecules. It also occurs as the product $k_\text{srxn}\ C_{[\text{O}]}$ and the two components cannot be individually determined.

Fig. 5 also shows the calculated parameter-optimized curves and experimental CO_2 response curves in response to input pulses of CO_2/Ar between 293 and 423 K. The influence of the temperature indicated that the adsorption of CO_2 was not activated and only the desorption of CO_2 depended on the reaction temperature. As the temperature increased, the desorption rate of CO_2 increased until above 423 K, it was faster than can be measured with the TAP technique, that is, the response curve was similar to the curve with no adsorption. The adsorption rate constant, and desorption activation energy and preexponential factor of the desorption rate constant of CO_2 were obtained from the curve fitting and listed in Table 1.

In reactions (5)–(7), the formation of CO_2 occurs as a consecutive reaction of adsorbed CO and the lattice oxygen of the catalyst. The rates of the adsorption, desorption and surface oxidation reaction of CO were estimated by fitting simulated curves to the experimental CO and CO_2 response curves that resulted from injected pulses of CO/Ar. The fit between the

Table 1
Estimated kinetic parameters for CO oxidation over 1.0% Ag/MnO_x

Parameter	Estimated value
D_{Ar} (m^2/s))	0.24×10^{-3}
$k_{ads,CO}$ C^0 (m^3 kg^{-1} s^{-1})	5.4
E_{CO} (kJ mol^{-1})	82.7
A_{CO} (s^{-1})	2.62×10^{11}
$k_{ads,CO_2} \cdot C^0$ (m^3 kg^{-1} s^{-1})	16.6
E_{CO_2} (kJ mol^{-1})	31.3
A_{CO_2} (s^{-1})	6.07×10^7
E_{srxn} (kJ mol^{-1})	115.6
A_{srxn} $C_{[O]}$ (s^{-1})	3.37×10^{12}

experimental and simulated curves is shown Fig. 6. The fitted kinetic parameters for the reactions of CO are listed in Table 1.

From Table 1, some important characteristics of the reaction can be deduced. First, adsorption of CO and CO_2 are not activated. Desorption of CO and CO_2 are fast even at 323 K, which implies desorption is not the determining step for the reaction mechanism on 1.0% Ag/MnO_x catalyst. The rate constants indicate that the rate of surface reaction is slower than the rate of CO adsorption at lower temperatures, that is, the former is the slow step in the mechanism. As the reaction temperature increases, the rate of the surface reaction increases until it is faster than the adsorption rate of CO and is no longer the rate controlling step above 493 K. The mechanism has different slow steps in different temperature regions.

3.5. Oxygen-assisted CO adsorption

The effect of coadsorbed O_2 on CO adsorption was also studied by the TAP technique. This can be done by pump-probe experiments or by first preadsorbing O_2 and then pulsing CO over an O_2 covered surface. Fig. 7 shows some results from the latter type of experiments.

In Fig. 7, it can be seen that for the room temperature CO pulse experiments, the CO response curve from the 1.0% Ag/MnO_x catalyst with preadsorbed O_2 was clearly shifted in time compared to the CO response curve from the catalyst without preadsorbed O_2. The shape of curve A is characteristic of fast adsorption, that is, it is due to multiple adsorption–desorption cycles. This indicated that coadsorbed O_2 promotes the adsorption of CO on the surface of the catalyst. This deduction was further supported by the following evidence. Response curves with a similar shape to curve A from CO pulses were only observed below 353 K and above 623 K. From TPD experiments [28], it is known that O_2 begins to desorb from the 1.0% Ag/MnO_x catalyst above 353 K and that some lattice oxygen gets converted to adsorbed oxygen and begins to desorb above 623 K. Between 353 and 623 K, the CO response curves of CO pulses over an O_2 preadsorbed surface and a clean surface are the same, as shown by that curves C and D in Fig. 7 from pulsing at 393 K are quite similar. In this temperature range, O_2 desorption is fast but lattice oxygen does not convert to adsorbed oxygen and the surface would be quite clean even with preadsorbed O_2 because this desorbs before the CO pulse.

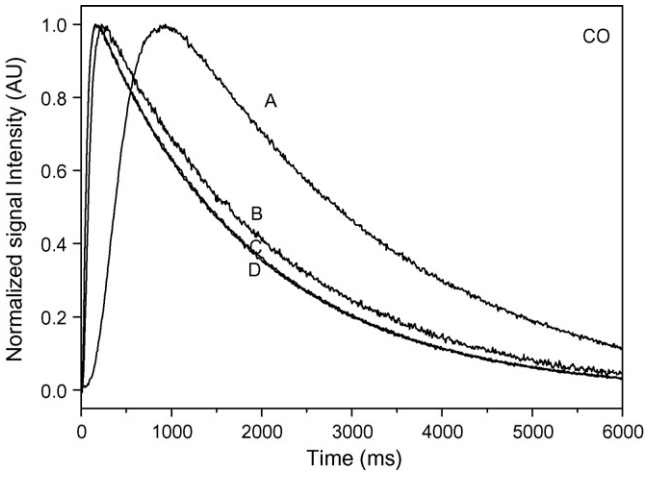

Fig. 7. CO response curves from CO/Ar pulsed over the 1% Ag/MnO_x catalyst. (A) 298 K, with preadsorbed O_2; (B) 298 K, without preadsorbed O_2; (C) 393 K, with preadsorbed O_2; and (D) 393 K, without preadsorbed O_2.

To confirm the existence of an oxygen-assisted CO adsorption phenomenon on the 1.0% Ag/MnO_x catalyst, the adsorption rate constants of CO adsorption in the two situations of CO adsorption (1) with preadsorbed oxygen and (2) a clean surface were estimated by curve fitting. The results are shown in Fig. 8 and Table 2, and show that there is a sharp increase, by about one order of magnitude, in the adsorption rate constant of CO due to coadsorbed O_2. There are some deviations between the experimental and simulated curves, which indicate that the adsorption–desorption steps are now more complicated than the simple scheme used here. No effort was made to get a better fit by adding more reaction steps because we do not yet have more direct evidence for these. Even so, the main qualitative feature of the experimental curves, that is, the shift of the curve maximum to a later time, was clearly reproduced.

At the same time, no CO_2 response was detected at the outlet of the reactor from CO pulsing at room temperature, which indicated that coadsorbed O_2, which promotes a fast CO

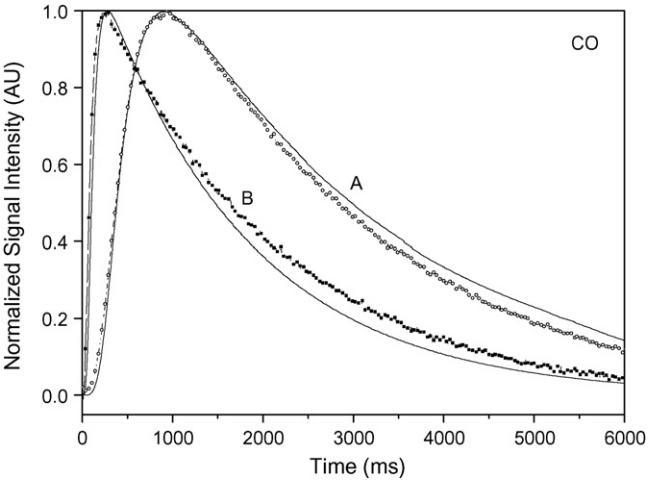

Fig. 8. Experimental (symbols) and simulated (lines) CO response curves to pulsed CO/Ar over the 1% Ag/MnO_x catalyst at 298 K. (A) with preadsorbed O_2 and (B) without preadsorbed O_2.

Table 2
Effect of pre-adsorbed oxygen on the CO adsorption rate constant at 298 K over 1.0% Ag/MnO_x

	Parameter	Estimated value
CO adsorption without coadsorbed O_2	$k_{ads,CO}$ ($m^3\,kg^{-1}\,s^{-1}$)	5.4
	$k_{des,CO}$ (s^{-1})	1.51
CO adsorption with coadsorbed O_2	$k_{ads,CO}$ ($m^3\,kg^{-1}\,s^{-1}$))	48.5
	$k_{des,CO}$ (s^{-1})	1.51

adsorption, does not promote CO oxidation. A possible reason is that at this low temperature, it is the rate of surface reaction that is the rate controlling step for the whole reaction, as discussed with the results in the previous sub-section. When the rate of surface reaction is too slow to produce detectable CO_2, an increase in the rate of CO adsorption will not necessarily produce detectable CO_2 at 298 K.

4. Conclusions

A MnO_x catalyst prepared by the reflux method had the typical structure of cryptomelane (OMS-2). This catalyst was loaded with different amounts of Ag. The loaded Ag metal was well dispersed in the micropores of the MnO_x OMS-2. The Ag/MnO_x catalysts showed excellent CO oxidation activity. Kinetic parameters for the elementary steps in CO oxidation were determined by curve fitting the response curves of single pulse TAP experiments on a 1.0% Ag/MnO_x catalyst. The activation energies were 83 kJ/mol for CO desorption, 31 kJ/mol for CO_2 desorption, and 116 kJ/mol for CO oxidation by lattice oxygen. The surface reaction is the rate controlling step at low temperature, but was not rate controlling above 493 K. Oxygen coadsorption promotes CO adsorption and increased the adsorption rate constant of CO adsorption about 10 times.

Acknowledgements

This work was supported by the Ministry of Science and Technology (No. G1999022408), the National Natural Science Foundation (No. 20773075) and Changde Cigarette Manufacture Company.

References

[1] H. Over, M. Muhler, Prog. Surf. Sci. 72 (2003) 3.
[2] R.J.H. Grisel, J.J. Slyconish, B.E. Nieuwenhuys, Top. Catal. 16/17 (2001) 425.
[3] M. Haruta, T. Kobayashi, H. Sano, N. Yamada, Chem. Lett. (1987) 405.
[4] M. Haruta, N. Yamada, T. Kobayashi, S. Iijima, J. Catal. 115 (1989) 301.
[5] G.C. Bond, D.T. Thompson, Gold Bull. 33 (2000) 41.
[6] M. Valden, X. Lai, D.W. Goodman, Science 281 (1998) 1647.
[7] D.R. Rolison, Science 299 (2003) 1698.
[8] S.B. Kanungo, J. Catal. 58 (1979) 419.
[9] L.S. Puckhaber, H.R. Cheung, D.L. Cocke, A. Clearfield, Solid State Ionics 32/33 (1989) 206.
[10] G.G. Xia, Y.G. Yin, W.S. Willis, J.Y. Wang, S.L. Suib, J. Catal. 185 (1999) 91.
[11] S.H. Taylor, C. Rhodes, Catal. Today 30 (2006) 357.
[12] A. Wootsch, C. Descorme, S. Rousselet, D. Duprez, C. Templier, Appl. Sur. Sci. 253 (2006) 1310.
[13] P. Thormählen, M. Skoglundh, E. Fridell, B. Andersson, J. Catal. 188 (1999) 300.
[14] J.D. Alexander, A.L. Christine, Appl. Catal. B: Environ. 67 (2006) 52.
[15] H. Fornander, L.G. Ekedahl, H. Dannetun, Surf. Sci. 441 (1999) 479.
[16] A.C. Boucher, V. Le Rhun, F. Hahn, N.A. Vante, J. Electroanalytical Chem. 555 (2003) 379.
[17] G.C. Bond, Catal. Rev. Sci. Eng. 41 (1999) 319.
[18] M.M. Slinko, E.S. Kurkina, M.A. Liauw, N.I. Jaeger, J. Chem. Phys. 111 (1999) 8105.
[19] N.M. Gupta, A.K. Tripathi, J. Catal. 187 (1999) 343.
[20] N.M. Gupta, A.K. Tripathi, Gold Bull. 34 (2001) 120.
[21] M. Olea, M. Kunitake, T. Shido, Y. Iwasawa, Phys. Chem. Chem. Phys. 3 (2001) 627.
[22] M. Olea, Y. Iwasawa, Bull. Chem. Soc. Jpn. 74 (2001) 255.
[23] R.J.H. Grisel, B.E. Nieuwenhuys, J. Catal. 199 (2001) 48.
[24] W.J. Li, Y. Wang, D.Z. Wang, F. Wei, Chin. J. Catal. 27 (2006) 200.
[25] J.T. Gleaves, J.R. Ebner, T.C. Kuechler, Catal. Rev. Sci. Eng. 30 (1988) 49.
[26] D.Z. Wang, Z.L. Li, C.R. Luo, W.Z. Weng, H.L. Wan, Chem. Eng. Sci. 58 (2003) 887.
[27] D.Z. Wang, F.X. Li, X.L. Zhao, Chem. Eng. Sci. 59 (2004) 5615.
[28] R.R. Hu, C. Yi, L.Y. Xie, D.Z. Wang, Chin. J. Catal. 28 (2007) 453.